This article has been accepted for publication in a future issue of this journal, but has not been fully edited. Content may change prior to final publication. Citation information: DOI 10.1109/TIA.2018.2810263, IEEE Transactions on Industry Applications

Single Stage PV Array Fed Speed Sensorless Vector Control of Induction Motor Drive for Water Pumping

Saurabh Shukla and Bhim Singh, *Fellow, IEEE*

***Abstract*—This paper deals with a single stage solar powered speed sensorless vector controlled induction motor drive for water pumping system, which is superior to conventional motor drive. The speed is estimated through estimated stator flux. The proposed system includes solar photovoltaic (PV) array, a three-phase voltage source inverter (VSI) and a motor-pump assembly. An incremental conductance (*InC*) based MPPT (Maximum Power Point Tracking) algorithm is used to harness maximum power from a PV array. The smooth starting of the motor is attained by vector control of an induction motor. The desired configuration is designed and simulated in MATLAB/Simulink platform and the design, modeling and control of the system, are validated on an experimental prototype developed in the laboratory.**

Keywords— Speed Sensorless Control, Stator Field-Oriented Vector Control, Photovoltaic (PV), InC MPPT Algorithm, Induction Motor Drive (IMD), Water Pump.

I. INTRODUCTION

In the modern era of development, renewable resources of energy, are being advocated by many countries to meet the increasing demand of electrical energy due to rapid depletion of non-renewable resources [1]-[2]. Solar PV based energy generation, has come up as an important alternative for many purposes [3]. The irrigation sector is one of the major sectors where solar PV power is extensively used for water pumping [4-5]. Solar PV water pumping has been initially realized using the DC motor. However, with all due virtues associated with the induction motor in terms of mechanical simplicity, ruggedness, reliability, low cost, higher efficiency and lower maintenance than the DC motors, it has replaced DC motors. Here, a solar PV array fed induction motor drive using vector control is used [6]-[7]. As one knows that solar PV power depends on solar insolation and temperature. The characteristic of PV module exhibits a single power peak. An extraction of maximum power is very important part of the PV system. Therefore, various MPPT (Maximum Power Point tracking) techniques have been developed and explained in the literature. These algorithms vary in their speed, range of effectiveness and complexities [8]. Here, an incremental conductance (*InC*) based MPPT algorithm is used to track MPPT. This algorithm is developed to overcome some drawbacks of perturb and observe (P&O) algorithm. *InC* algorithm improves the tracking time and to produce increased energy on a vast irradiation changes. Moreover, it has advantage over P&O method, which increases losses in slow varying atmospheric condition as it oscillates around MPP [9]-[10].

Most of the existing induction motor drives (IMDs) incorporate one DC-DC converter and a VSI (Voltage Source Inverter) for achieving MPPT and maximum efficiency of the motor [11]. Moreover, the DC link voltage regulation is achieved by VSI itself. However, the system requires at least seven power converter switches and hence switching losses are increased. This further includes a DC-AC conversion with a VSI feeding a vector-controlled three-phase IMD. Therefore, there is a need to use single stage controlled drive for water pumping and thereby decreasing number of switches and losses. In single stage system, a VSI has to maintain the MPP as well as DC link voltage is also controlled by it. Therefore, variable DC link voltage cannot be achieved as explained in [12]-[13].

The vector control strategy is superior to scalar control in terms of speed of response and accuracy as explained in [14]-[16]. In the vector control technique, an AC motor is operated in such a manner to behave dynamically as a DC motor by using feedback control [16]. This technique enables to vary the speed over the wide range. Hence with the advancement of power electronics and by using powerful microcomputer and DSPs, the vector control ousts scalar control [17]-[19]. In this vector control scheme, the stator flux is estimated in stationery αβ frame, which is used to estimate the slip speed (ω_{sl}), synchronous speed (ω_e) and the motor speed as explained in [20]. The paper is organized as given: system configuration is given in section II followed by the design of system, control strategy including vector control and results and discussion in the subsequent sections. The performance of the given system is achieved through simulation using MATLAB/Simulink. Simulation results are validated by experimentation carried out in the laboratory on the developed prototype.

II. SYSTEM CONFIGURATION

Fig.1 shows the configuration of a single stage solar PV array fed speed sensorless induction motor drive incorporating vector control for water pumping. This proposed system constitutes PV array followed by a VSI fed three-phase induction motor drive operated pump. The motor speed is estimated by stator fluxes, which is estimated by DC link voltage and motor currents. Three-phase VSI switching is controlled by hysteresis-band controller. An incremental conductance (InC) control algorithm is used for MPPT to generate switching pulses for the VSI.

III. SYSTEM DESIGN

Fig.1 shows a basic schematic of a three-phase induction motor of a 7.5 kW (10 HP), 415V, used to drive the pump powered by a 8.7 kW maximum power solar PV array. The various stages of system, have been designed here and the performance of overall system is shown in subsequent sections under various conditions. The detailed data are given in Appendices.

This article has been accepted for publication in a future issue of this journal, but has not been fully edited. Content may change prior to final publication. Citation information: DOI 10.1109/TIA.2018.2810263, IEEE Transactions on Industry Applications

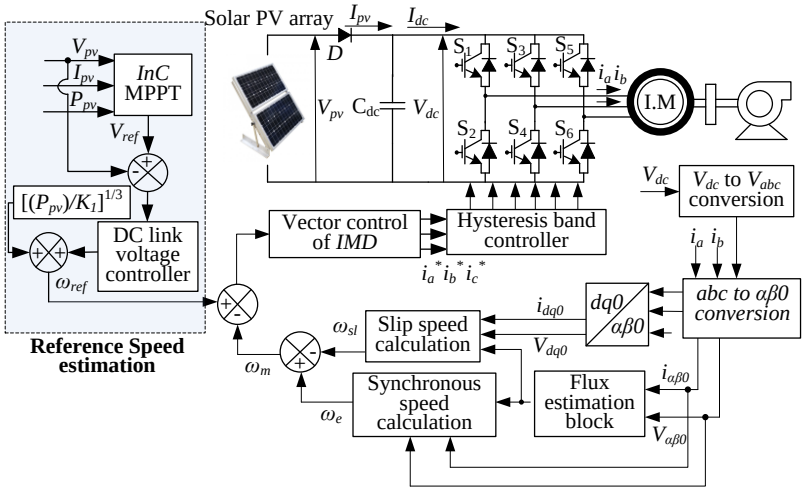

Fig. 1. PV fed induction motor drive configuration

A. Design of Solar PV Array

A 8700 W PV array is designed to drive a 7.5kW induction motor drive. The rating of PV array is selected more than the motor rating so that the performance of the motor remains unaffected by the losses incurred in the motor and converter. A PV array is designed by connecting 34 PV modules in series of open circuit voltage (V_{oc}) equals 734V and 25 modules in parallel of short circuit current (I_{sc}) equal to 15.5 A, respectively. The voltage and current reach their MPP on about 81% of V_{oc} and 90% of I_{sc} respectively as given in Table I. The specifications of PV module used, are given in Table II and in Appendices.

TABLE I PV ARRAY DESIGN (SIMULATION DATA)

MPP voltage, V_{mp}	600V
MPP power, P_{mp}	8700W
MPP current, I_{mp}= P_{mp}/V_{mp}	14.5A
Number of module in series, N_{ser}= V_{mp}/V_{mpp}	34
Number of module in parallel, N_{par}=I_{mp}/I_{mpp}	25

TABLE II PV MODULE (SIMULATION DATA)

V_{oca} of one module	21.6V
I_{sca} of one module	0.64A
MPP Voltage, V_{mpp}	0.81*21.6=17.6V
MPP Current, I_{mpp}	0.9*0.64=0.58A

B. Calculation of DC Link Voltage

In order to control the output current of VSI, the voltage of the DC link should be more than as compared to the peak amplitude of line voltage given to the motor [13].

$$V_{dc} = \sqrt{2} \times V_L = \sqrt{2} \times 415 = 587V \quad (1)$$

Hence the value of DC link voltage is kept as 600V.

C. Design of DC Link Capacitor

The value of DC link capacitor is estimated by using fundamental frequency component as [13],

$$\omega_{rated} = 2 \times \pi \times f_{rated} = 2 \times \pi \times 50 = 314 rad/s \quad (2)$$

$$\frac{1}{2} \times C_{dc} \times \left(V_{dc}^2 - V_{dc1}^2\right) = 3aV_p It = 3 \times 1.2 \times 239.6 \times 13.5 \times .005 \quad (3)$$

Hence, C_{dc}= 2509μF

where V_{dc} is the DC link voltage and V_{dc1} is the minimum allowable DC link voltage during transient condition, t is the time required for the voltage to recover minimum allowable DC-link voltage, I is the motor phase current and V_p is the phase voltage. Therefore, capacitor value is selected as 2500 μF.

D. Design of Water Pump

Water pumps have non-linear relationship between load torque and motor speed [21] i.e. load torque *(T_L)* is directly in proportion to the square of the rated rotor speed. Hence,

$$T_L = K_1 \omega_m^2 \quad (4)$$

where K_1 is the proportionality constant of the pump.

IV. CONTROL OF RECOMMENDED SYSTEM

The control of overall system includes MPPT of solar PV array to extract maximum power through three phase VSI, control of three-phase VSI switching by using hysteresis-band controller for vector-controlled IMD and speed estimation for speed sensorless vector control of an induction motor drive.

A. Incremental-Conductance Algorithm

The technique for controlling the PV array voltage is given in Fig.2. There is a nonlinear relationship between power and voltage in solar PV array characteristic and various MPPT techniques have been used to track maximum power point. However, because of its inherent demerit of oscillation at MPP and loss associated with *P&O* technique as discussed in previous section, an *InC* control algorithm is used. The commanding equations for explaining the operating principle of *InC*, are given as,

$$P_{pv} = V_{pv} * I_{pv} \quad (5)$$

$$\frac{\Delta P_{pv}}{\Delta V_{pv}} = I_{pv} + V_{pv} * \frac{\Delta I_{pv}}{\Delta V_{pv}} = 0 \quad (6)$$

$$\frac{\Delta I_{pv}}{\Delta V_{pv}} = -\frac{I_{pv}}{V_{pv}} \quad (7)$$

This article has been accepted for publication in a future issue of this journal, but has not been fully edited. Content may change prior to final publication. Citation information: DOI 10.1109/TIA.2018.2810263, IEEE Transactions on Industry Applications

where V_{pv} and I_{pv} are the instantaneous voltage and current values.

The reference voltage V_{ref} is bonded between upper and lower limit set between $0.9V_{oc}$-$0.8V_{oc}$. In case, if V_{ref} does not lie within the boundary, it is set to its nearest saturated value. From the above equation, it is clear that on the left side of MPP the slope is positive meaning $\Delta I_{pv}/\Delta V_{pv} > (-I_{pv}/V_{pv})$ and on the right side of MPP the slope is negative, which implies $\Delta I_{pv}/\Delta V_{pv} < (-I_{pv}/V_{pv})$ and slope at MPP should be zero as shown in Fig.2.

Fig.3 shows the method of perturbation using *InC* based MPP algorithm.

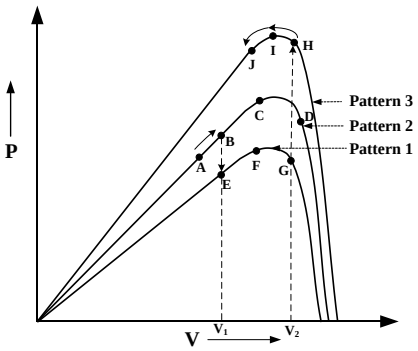

Fig. 2. P_{pv}-V_{pv} curve for one module

The inputs to the MPPT algorithm, are PV voltage and current. The reference PV voltage, thus obtained at k^{th} sampling instant, is the reference DC link voltage V_{dc}^{*} and it is compared with the PV voltage as,

$$V_{dcl(k)} = V_{dc(k)}^{*} - V_{pv(k)} \quad (8)$$

Fig.4 (a) shows the schematic for the generation of error signal $V_{dcl(k)}$, which is fed to DC link voltage PI controller and the resulting speed error signal at the k^{th} sampling instant and is given as follows,

$$\omega_{1(k)} = \omega_{1(k-1)} + K_{pdc}\left\{V_{dcl(k)} - V_{dcl(k-1)}\right\} + K_{idc}V_{dcl(k)} \quad (9)$$

Fig.4 (b) shows the PV power converted into a speed term by the following relation and this gives one component of the reference speed by affinity law of pump. It can be treated as the feed forward component.

The physical significance of ω_2 quantity can be justified as maximum rated speed corresponding to the given insolation. Only PI controller pushes the voltage error to the desired reference speed (ω_{ref}). However, the dynamic response of the system becomes very poor. It can be seen from the feed forward term that it consists of P_{pv} and the proportionality constant obtained from motor affinity law. Both of these terms help in fast dynamic response by instantaneously reflecting the PV power on motor speed. It is expressed by the following formula.

$$P_{pv} = K_1\omega_2^3 \quad (10)$$

where K_1 is proportionality constant of pump obtained in (4).

Hence, the reference speed of the motor is estimated as,

$$\omega_{ref} = \omega_1 + \omega_2 \quad (11)$$

This reference speed is used for control of VSI feeding induction motor drive.

TABLE III MPPT THROUGH INC ALGORITHM DURING INSOLATION VARIATION

Atmospheric condition	Current Point → Next point	Electrical quantity	Duty cycle
Fixed Solar Insolation (Pattern 2)	A→B	P↑ V↑	$V_{dc}^{*}+\Delta V_{pv}$
	B→C	P↑ V↑	$V_{dc}^{*}+\Delta V_{pv}$
	C→D	P↓ V↑	$V_{dc}^{*}+\Delta V_{pv}$
	D→C	P↑ V↓	$V_{dc}^{*}-\Delta V_{pv}$
	C→B	P↓ V↓	$V_{dc}^{*}-\Delta V_{pv}$
At point 'B', insolation changed New operating point is 'E'			
New Insolation level (Pattern 1)	E→F	P↑ V↑	$V_{dc}^{*}+\Delta V_{pv}$
	F→G	P↓ V↑	$V_{dc}^{*}+\Delta V_{pv}$
	G→F	P↑ V↓	$V_{dc}^{*}-\Delta V_{pv}$
	F→E	P↓ V↓	$V_{dc}^{*}-\Delta V_{pv}$
	E→F	P↑ V↑	$V_{dc}^{*}+\Delta V_{pv}$
	F→G	P↓ V↑	$V_{dc}^{*}+\Delta V_{pv}$
At point 'G', insolation changed New operating point is 'H'			
New Insolation level (Pattern 3)	H→I	P↑ V↓	$V_{dc}^{*}-\Delta V_{pv}$
	I→J	P↓ V↓	$V_{dc}^{*}-\Delta V_{pv}$
	J→I	P↑ V↑	$V_{dc}^{*}+\Delta V_{pv}$
	I→H	P↓ V↑	$V_{dc}^{*}+\Delta V_{pv}$

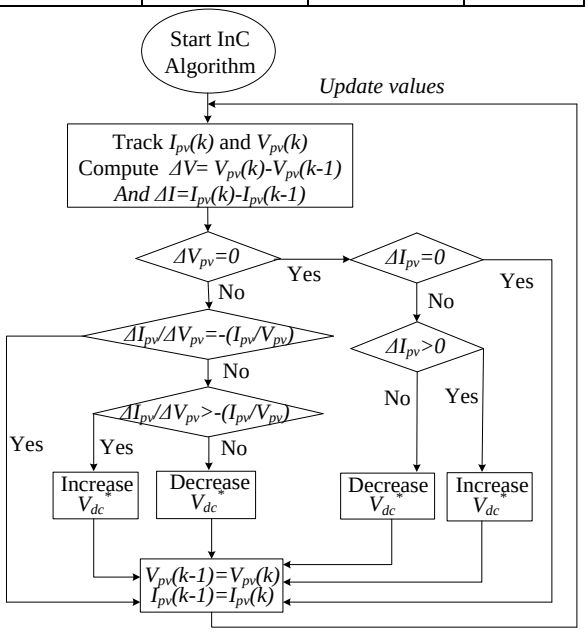

Fig. 3. Incremental-Conductance algorithm

B. Speed Estimation of Induction Motor Drive

The fundamental equations for the estimation of speed are given as follows.

The three phase VSI voltages (v_a, v_b, v_c) are obtained by the DC link voltage (V_{dc}) by the expression as,

$$v_a = \frac{V_{dc}}{3}*\left(2S_a - S_b - S_c\right), v_b = \frac{V_{dc}}{3}*\left(2S_b - S_a - S_c\right)$$

$$v_c = \frac{V_{dc}}{3}*\left(2S_c - S_b - S_a\right) \quad (12)$$

where S_a, S_b and S_c are switching functions (which are either one or zero) of VSI.

The various voltage and current transformation equations to transform from *abc* to *αβ* domain are given as,

This article has been accepted for publication in a future issue of this journal, but has not been fully edited. Content may change prior to final publication. Citation information: DOI 10.1109/TIA.2018.2810263, IEEE Transactions on Industry Applications

$$v_\alpha = \frac{1}{3}\left(2v_a - v_b - v_c\right), v_\beta = \sqrt{3}\left(v_b - v_c\right) \quad (13)$$

$$i_\alpha = \frac{1}{3}\left(2i_a - i_b - i_c\right), i_\beta = \sqrt{3}\left(i_b - i_c\right) \quad (14)$$

where i_a, i_b, i_c are balanced three phase winding currents.

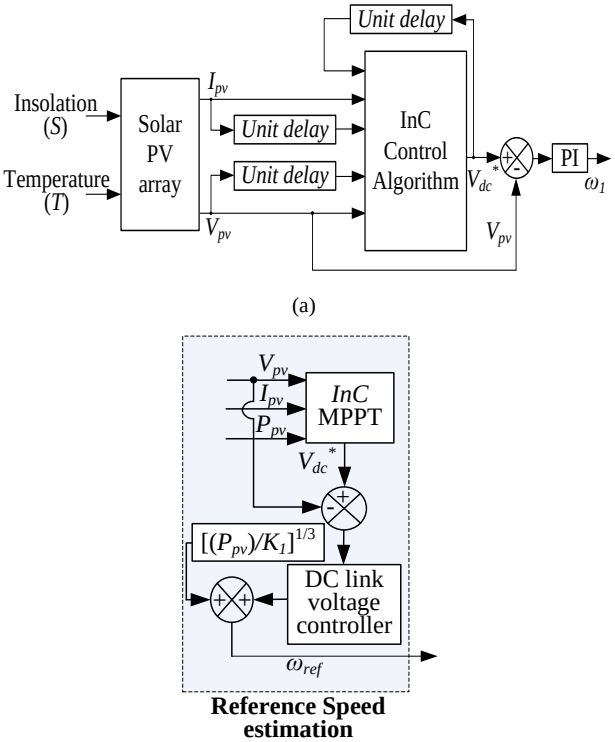

Fig. 4. Reference speed generation (a) ω_1 estimation (b) Feed-forward speed component

This transformation is applicable for all rotating variables viz. voltage, current and flux quantities. The stationery components of flux are given as,

$$\frac{d}{dt}\left(\psi_\beta\right) = \left(v_\beta - R_s * i_\beta\right), \frac{d}{dt}\left(\psi_\alpha\right) = \left(v_\alpha - R_s * i_\alpha\right) \quad (15)$$

$$\psi_s = \sqrt{\psi_\alpha^2 + \psi_\beta^2} \quad (16)$$

$$i_{qs} = i_\beta \times \frac{\psi_\alpha}{\psi_s} - i_\alpha \times \frac{\psi_\beta}{\psi_s} \quad (17)$$

$$i_{ds} = i_\beta \times \left(\psi_\beta / \psi_s\right) + i_\alpha \times \left(\psi_\alpha / \psi_s\right) \quad (18)$$

$$\psi_{ds} = \psi_\beta \times \left(\psi_\beta / \psi_s\right) + \psi_\alpha \times \left(\psi_\alpha / \psi_s\right) \quad (19)$$

$$\omega_e = \frac{\left(V_\beta - R_s * i_\beta\right)\psi_\alpha - \left(V_\alpha - R_s * i_\alpha\right)\psi_\beta}{\psi_s^2} \quad (21)$$

where i_{ds} and i_{qs} are current components in synchronously rotating *dq0* frame, $\sigma = 1 - L_m^2 / \left(L_s * L_r\right)$, $\tau_r = L_r / R_r$, L_r=rotor inductance, L_m=magnetizing inductance, L_{lr}= rotor leakage inductance, L_{ls}= stator leakage inductance, R_r=stator referred rotor resistance, R_s=stator resistance.

The motor rotational speed is given as,

$$\omega_m = \omega_e - \omega_{sl} \quad (22)$$

The slip speed (ω_{sl}) and synchronous speed (ω_e) are estimated as,

$$\omega_{sl} = \frac{\left(1 + \sigma S \tau_r\right) L_s i_{qs}}{\tau_r \left(\psi_d - \sigma L_s i_{ds}\right)} \quad (20)$$

C. Field-Weakening Control

The relationship of direct axis current with speed (ω_m) at a given base speed of the motor (ω_{base}) is given below,

$$I_{dm}^{e*} = I_{mag} \quad \text{(for } \omega_m \leq \omega_{base}\text{)} \quad (23)$$

$$I_{dm}^{e*} = \frac{\omega_{base}}{\omega_m} I_{mag} \quad \text{(for } \omega_m > \omega_{base}\text{)} \quad (24)$$

where I_{mag} is the magnetizing current of the motor.

D. Vector Control of Induction Motor Drive

Fig.5 shows the schematic of vector control method, which is used to control the stator currents and flux. It comprises of three stages.

The flux component of current vector (I_{dm}^*) is calculated as,

$$I_{dm}^* = I_{dm}^{e*} + \tau_r \times \frac{d}{dt} I_{dm}^{e*} \quad (25)$$

During steady-state condition, the derivative term tends to zero.

The reference flux component (ψ_{ds}^*) is calculated as,

$$\psi_{ds}^* = L_m I_{dm}^{e*} \quad (26)$$

The flux error is passed through flux PI controller, which pushes the error signal to zero and the output is the exciting current (I_{ds}^*). The involved equations are given as,

$$\psi_e = \psi_{ds}^* - \psi_{ds} \quad (27)$$

$$I_{ds(k)}^* = I_{ds(k-1)}^* + K_{p\psi}\left\{\psi_{e(k)} - \psi_{e(k-1)}\right\} + K_{i\psi}\psi_{e(k)} \quad (28)$$

Some decoupling effect is present in vector control, due to which the change is torque component of current (i_{qs}) can change the torque as well as flux. Therefore, this effect must be eliminated by adding one feed-forward path. The equation of decoupling component of current is given as,

$$I_{dcp} = \frac{\sigma \tau_r \omega_{sl} i_{qs}}{1 + \sigma S \tau_r} \quad (29)$$

Therefore, the final expression for exciting component of current is given as,

$$I_{ds}^{e*} = I_{ds}^* + I_{dcp} \quad (30)$$

The torque component of current vector (I_{qs}^{e*}) is calculated as follows,

The desired speed (ω_{ref}) and estimated speed (ω_m) is compared and the error is passed through speed PI controller to generate reference torque ($T_{e(k)}^*$) as,

$$\omega_{error} = \omega_{ref} - \omega_m \quad (31)$$

$$T_{e(k)}^* = T_{e(k-1)}^* + K_{p\omega}\left\{\omega_{error(k)} - \omega_{error(k-1)}\right\} + K_{i\omega}\omega_{error(k)} \quad (32)$$

$$I_{qs}^{e*} = T_e^* / \left(K \times I_{ds}^{e*}\right) \quad (33)$$

where $K = 3PL_m / 4L_r$, P is the number of poles.

The reference slip speed (ω_{sl}^*) is calculated as,

$$\omega_{sl}^* = I_{qs}^{e*} / \left(\tau_r * I_{ds}^{e*}\right) \quad (34)$$

This article has been accepted for publication in a future issue of this journal, but has not been fully edited. Content may change prior to final publication. Citation information: DOI 10.1109/TIA.2018.2810263, IEEE Transactions on Industry Applications

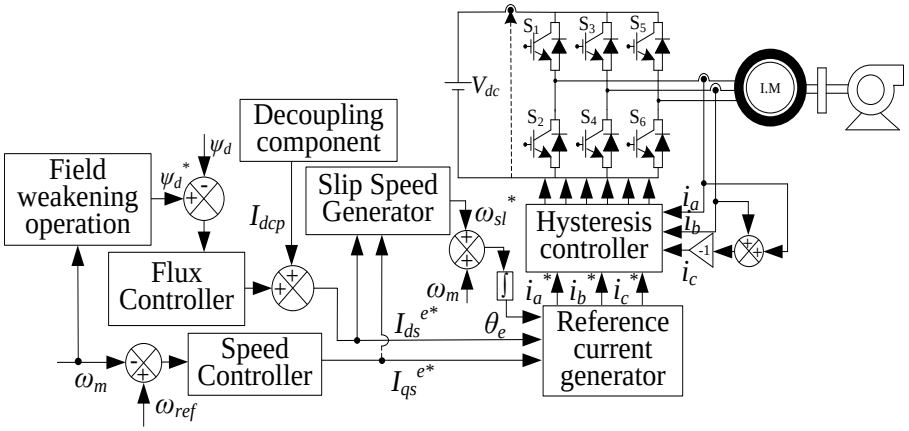

Fig. 5. Vector control of IMD

This reference slip speed (ω_{sl}^*) is added with the estimated speed (ω_m) to calculate reference synchronous speed (ω_e^*) in rad/s.

$$\omega_e^* = \omega_m + \omega_{sl}^* \tag{35}$$

The synchronous speed thus calculated is used to get flux-angle (θ_e) at the kth sampling instant as,

$$\theta_{e(k)} = \theta_{e(k-1)} + \omega_e^* \times T \tag{36}$$

where T=Sampling period of the signal.

The value of *q-axis* and *d-axis* current components ${I_{ds}}^{e*}$ and ${I_{qs}}^{e*}$ respectively obtained from (30) and (33), are used to obtain reference phase currents i_a^*, i_b^*, i_c^*, by following equations,

$$i_a^* = I_{ds}^{e*} \sin\theta_e + I_{qs}^{e*} \cos\theta_e \tag{37}$$

$$i_b^* = I_{ds}^{e*} \sin\left(\theta_e - 120^\circ\right) + I_{qs}^{e*} \cos\left(\theta_e - 120^\circ\right) \tag{38}$$

$$i_c^* = I_{ds}^{e*} \sin\left(\theta_e + 120^\circ\right) + I_{qs}^{e*} \cos\left(\theta_e + 120^\circ\right) \tag{39}$$

These phase currents (i_a^*, i_b^*, i_c^*) are compared with the sensed phase currents (i_a, i_b, i_c) and the error signal is passed through hysteresis-band controller to generate switching pulses for VSI.

V. Simulated Performance of the System

The proposed single stage solar PV fed vector controlled induction motor drive is modeled for water pumping and its simulation has been performed in MATLAB/Simulink using SPS toolbox. The salient points of these results are as follows.

A. Starting and Steady state Performance of the Drive

Fig.6 presents that the solar PV array parameters such as solar PV voltage (V_{pv}), PV current (I_{pv}), PV power (P_{pv}), DC link voltage (V_{dc}) which increases and settles at the MPP point within fraction of second. The reference speed (ω_{ref}) is calculated by adding speed derived from the voltage controller output (ω_1) and from P_{pv} i.e. (ω_2).The PV MPP is tracked by a well-known MPPT control algorithm i.e. *InC* and the excellent tracking profile is achieved during dynamically changing weather conditions. The perturbation size is adjusted to mitigate oscillations around MPP. Henceforth, smooth and stable starting performances of solar PV fed vector controlled induction motor drive at a fixed insolation of 1000W/m^2, are achieved. It is observed that soft starting is achieved by vector control of an induction motor first and within few seconds the steady-state condition is reached as the DC link voltage achieves its steady state value of 600V and the solar PV array achieves V_{mp} and I_{mp} at 0.1s. Fig.7 shows the estimation of motor speed (ω_m) from slip speed (ω_{sl}) and synchronous speed (ω_e) using estimated stationery flux components (ψ_α and ψ_β). The electromagnetic torque (T_e) achieves its steady-state value 24.54 Nm at 1000W/m^2 very quickly with a limit of 34 Nm (within allowable range) and the pump torque (T_p) quickly settles down to a steady-state value. Fig.8 (a) deals with the smooth and stable performance of the motor-pump and it has been observed that the motor steady state performance is achieved within fraction of second. Fig.8 (b) demonstrates the waveforms of sensed speed (ω_{sen}) and estimated speed (ω_m). It is observed that both speeds (ω_{sen} and ω_m) are matching during the steady state condition.

B. Dynamic Performance of Proposed System During Step Decrease in Variable Irradiance

Fig.9 and Fig.10 (a) show the satisfactory dynamic performance of the drive when insolation level is reduced from 1000W/m^2 to 500W/m^2 after 1s. From the *P-V* and *I-V* curve of PV array it is evident that there is normal change in the open circuit voltage (V_{oc}) and voltage at maximum power (V_{pv}) however, short circuit current (I_{sc}) and current at MPP (I_{pv}) change significantly. Once MPP is tracked, the control algorithm (*InC*) maintains it at that MPP. Fig.10 (b) shows that both the speeds (ω_{sen} and ω_m) track the reference value at steady state condition. There is slight delay in speed estimation during dynamic condition, which is due to the estimation of speed is achieved by fluxes, which depend upon the sensed parameters like DC link voltages and phase currents.

C. Dynamic Performance of Proposed System During Step Increase in Variable Irradiance

Fig.11 and Fig.12 (a) show the satisfactory performances of the system during variable insolation. The detailed explanation is given above and the behavior is verified by Fig.11 in which the insolation level is increased from 500W/m^2 to 1000 W/m^2 after 1.0 s and settles at 1000 W/m^2. The satisfactory motor-pump performance is observed during this variation in the insolation. Fig.12 (b) shows the waveforms of estimated and sensed speed (ω_{sen} and ω_m), which track the reference value

This article has been accepted for publication in a future issue of this journal, but has not been fully edited. Content may change prior to final publication. Citation information: DOI 10.1109/TIA.2018.2810263, IEEE Transactions on Industry Applications

obtained from the DC link voltage controller in steady state condition with slight deviation in insolation transition.

Table IV shows the steady-state performance of the drive in terms of PV voltage (V_{pv}), PV current (I_{pv}). DC link voltage (V_{dc}), THD_i (total harmonic distortion of motor current) for wide range of speed control as it is controlled and regulated by vector-controlled VSI fed IMD. THD_i increases as the insolation decreases.

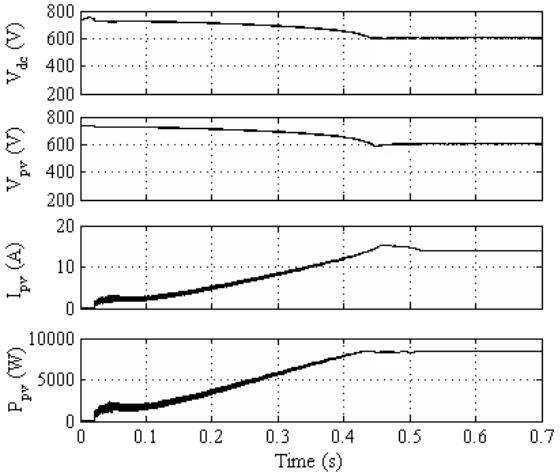

Fig. 6. Starting and MPPT of PV array at 1000 W/m^2

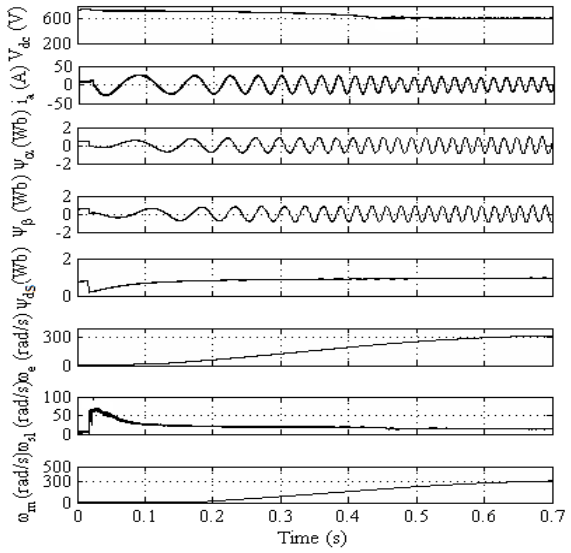

Fig. 7. Intermediate signals during starting at 1000 W/m^2

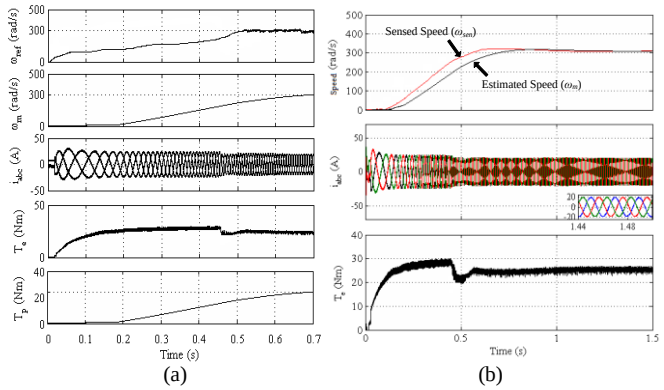

(a) (b)

Fig. 8. Simulation results during starting at 1000 W/m^2 (a) Proposed drive (b) Waveforms showing sensed speed and estimated speed

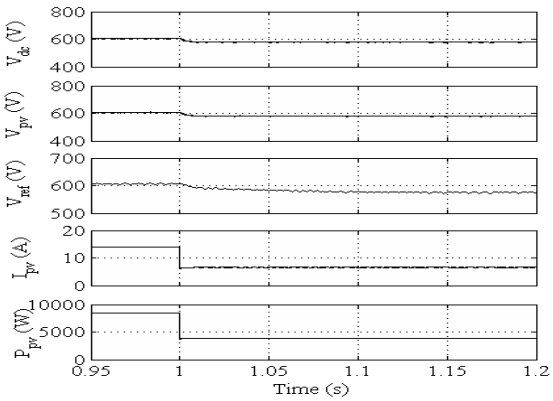

Fig. 9. SPV array performance during decrease in insolation from 1000 W/m^2 to 500 W/m^2

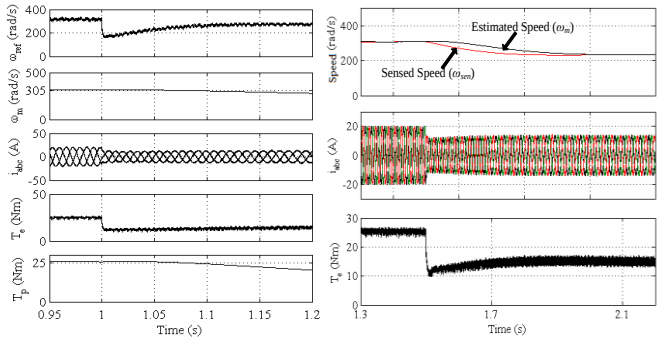

(a) (b)

Fig. 10. Dynamic performance during irradiance decrement from 1000 W/m^2 to 500 W/m^2 (a) Proposed drive (b) Waveforms showing sensed speed and estimated speed

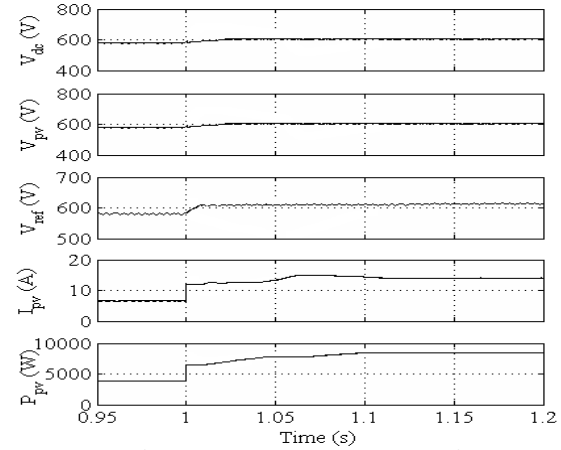

Fig. 11. PV array performance on increasing insolation from 500 W/m^2 to 1000 W/m^2

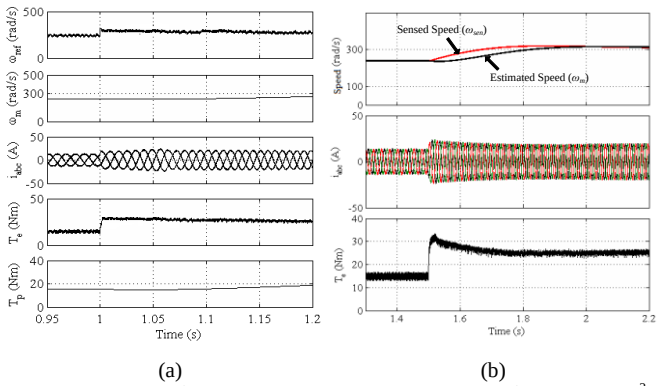

(a) (b)

Fig. 12. Dynamic performance during irradiance decrement from 500 W/m^2 to 1000 W/m^2 (a) Proposed drive (b) Waveforms showing sensed speed and estimated speed

This article has been accepted for publication in a future issue of this journal, but has not been fully edited. Content may change prior to final publication. Citation information: DOI 10.1109/TIA.2018.2810263, IEEE Transactions on Industry Applications

TABLE IV PERFORMANCE OF THE DRIVE AT DIFFERENT INSOLATION

Insolation (W/m^2)	P_{pv}(W)	V_{pv}(V)	I_{pv}(A)	Speed (rad/s)	Torque (Nm)	THD_i (%)
1000	8700	600	14.5	305	24.5	2.78
800	6610	595	11.05	289	20.5	3.06
600	4730	586	8.0	255	17	3.35
400	2900	570	5.08	220	11.8	4.16
200	1140	530	2.15	160	7	5.01

VI. EXPERIMENTAL VALIDATION

Fig. 13 demonstrates the block diagram representation of signal conditioning and control of proposed topology. The performances of the single stage PV array fed IM-pump assembly, are experimentally validated on a developed prototype in the laboratory, shown in Fig.14. Due to the laboratory constraints, the proposed system performance is validated on a 230V, 2200W, 4-pole, 1430rpm induction motor. The main components of proposed system comprise of a photovoltaic simulator (ETS600x17DPVF Terra SAS), three current sensors (LA-55P) and a voltage sensor (LV-25P). The characteristics of volumetric type water pump resemble the DC generator fed resistive load as it becomes comparable to volumetric pump when the armature voltage drop is neglected as the torque becomes proportional to speed. A VSI (SEMIKRON MD B6CI 600/415–35F), real-time DSP controller (dSPACE 1104) are used to perform the motor speed control. For recording purpose, a four-channel digital storage oscilloscope (Agilent make DSO) is used. The PWM signals from DSP, are in range of 0–5V and gate driver of the semiconductor switches requires 15-V signal. The transistor (2N2222) circuitry is used to pull up the PWM voltage to 15V required for the gate driver circuit of three-phase inverter. Opto-couplers (6N136) are used for providing isolation between the controller and gate driver circuit.

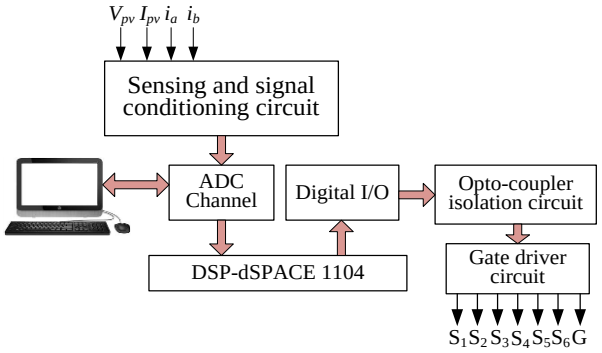

Fig. 13. Block diagram of signal conditioning and control architecture of test setup

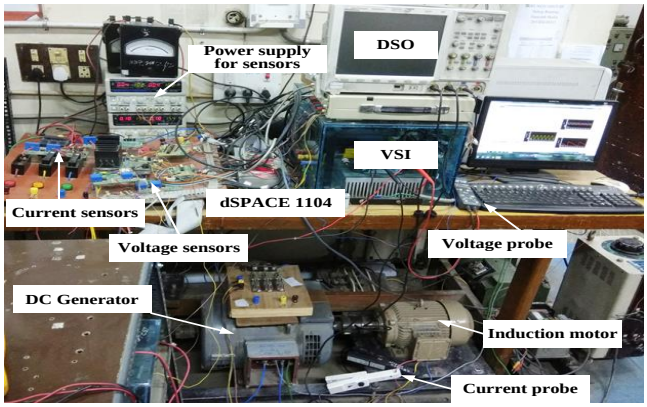

Fig. 14. Photograph of Experimental prototype of the proposed system

A. Test Results for MPPT

Figs.15 (a-b) show the excellent performance of the drive at two insolation level viz. 1000 W/m^2 and 500 W/m^2. The P_{pv}-V_{pv} and I_{pv}-V_{pv} curves shown at each insolation level, display the tracking efficiency nearly 100% in each case, which verifies the full utilization of solar PV power at rated condition as well as at reduced insolation.

B. Performance During Starting

Fig.16 (a) shows the soft starting of the drive at 1000 W/m^2. The MPP voltage (V_{pv}) is set at 350 V with the current at MPP (I_{pv}) fixed at 7.2 A. The MPP is tracked immediately after the motor is started. Test results shown in Fig.16, demonstrate PV voltage (V_{pv}), PV current (I_{pv}), stator phase current (i_a) and estimated motor speed in rpm (ω_m). The performance of the drive during starting is satisfactory and the parameters reach their steady-state value immediately after starting. Fig.16 (b) shows the waveforms of sensed speed (ω_{sen}) and estimated speed (ω_m), in which slight delay in ω_m is observed at starting. This is because, the estimation of speed is achieved from rotor fluxes, which depend on different sensing of parameters viz. DC link voltage and phase currents. Figs.17 (a-b) present the similar kind of observation at reduced irradiance (500 W/m^2). The performance indices show satisfactory results at rated as well as at reduced irradiance conditions.

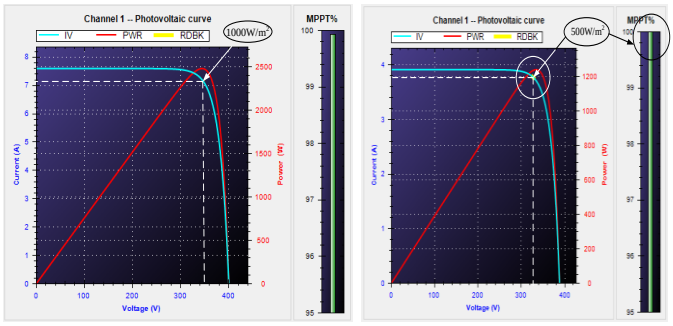

(a) (b)

Fig. 15. MPPT of SPV array (a) 1000W/m^2 (b) 500W/m^2

C. Performance in Steady State

Fig.18 (a-b) show the steady state performance of the drive in terms of PV voltage and three phase currents of the motor at 1000 W/m^2 and 500 W/m^2. It is observed that PV voltage is settled at MPP voltage and the three phase currents (i_a, i_b, i_c) are also at their rated value with 120° apart from each-other.

D. Dynamic Performance of Drive: Irradiance Decrement

Fig.19 (a) shows the performance of the drive during step decrement of variable insolation. The drive performance is exceptionally satisfactory as all the indices (viz. V_{pv}, I_{pv}, i_a and ω_m) are abided by the variation and follow the change. Fig. 19 (b) shows the waveforms, showing ω_{sen} and ω_m during dynamic condition. It is observed that the plot of estimated speed (ω_m) is slightly delayed under dynamic condition. However, it coincides with the sensed speed parameter (ω_{sen}) in steady state and the error speed signal (ω_{error}) is nearly zero in steady state condition.

Fig. 20 shows the intermediate signals in terms of internal fluxes and estimated speeds (ψ_α, ψ_β, ω_{sl}, ω_e). It is observed that the flux signals vary in their frequency as the irradiance is altered from 1000 W/m^2 to 500 W/m^2. The slip speed in rad/s (ω_{sl}) and the synchronous speed in rad/s (ω_e), are estimated by the formulae given in the previous section, are shown decreasing as the irradiance is decreased.

This article has been accepted for publication in a future issue of this journal, but has not been fully edited. Content may change prior to final publication. Citation information: DOI 10.1109/TIA.2018.2810263, IEEE Transactions on Industry Applications

E. Dynamic Performance: Increase in Irradiance

Similar performance is observed in Figs. 21 (a-b) and Fig.22, when the irradiance is changed from 500W/m^2 to 1000 W/m^2. It is observed that the proposed system's performance indices in terms of internal fluxes and estimated speeds (ψ_α, ψ_β, ω_{sl}, ω_e) comply with the change in environmental conditions being realized here in terms of change in irradiance. The estimated speeds show gradual change as the irradiance is changed from 500 W/m^2 to 1000 W/m^2.

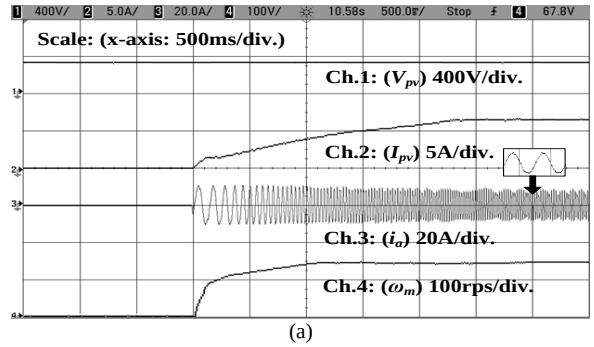

(a)

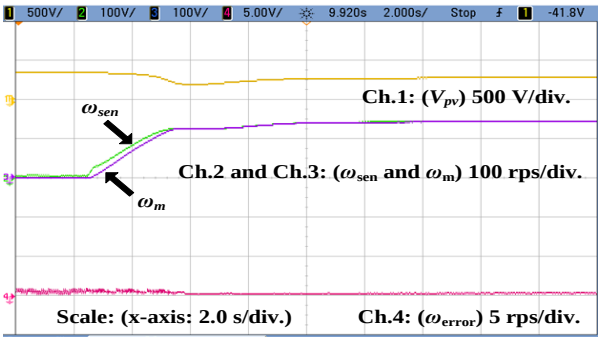

(b)

Fig. 16. Soft starting at 1000 W/m^2 irradiance (a) Performance of the proposed system (b) Waveforms showing sensed speed (ω_{sen}) and estimated speed (ω_m)

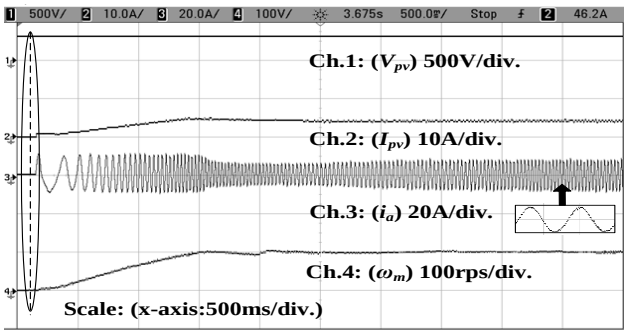

(a)

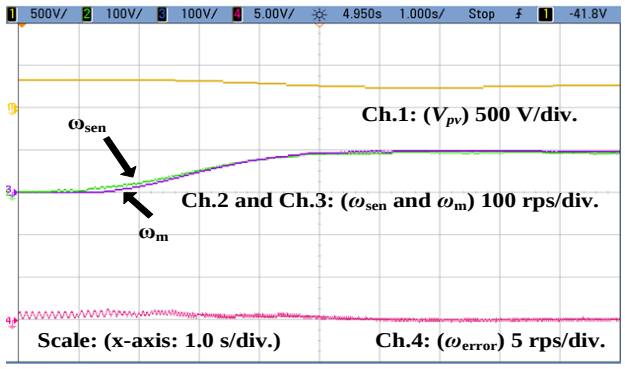

(b)

Fig. 17. Soft Starting at 500 W/m^2 irradiance (a) Performance of the proposed system (b) Waveforms showing sensed speed (ω_{sen}) and estimated speed (ω_m)

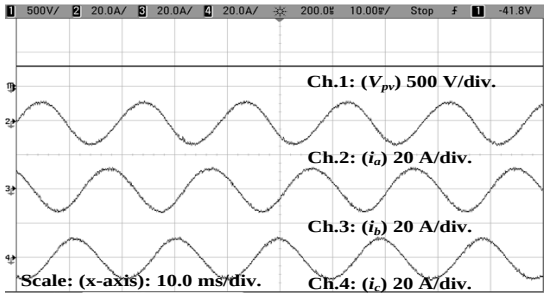

(a)

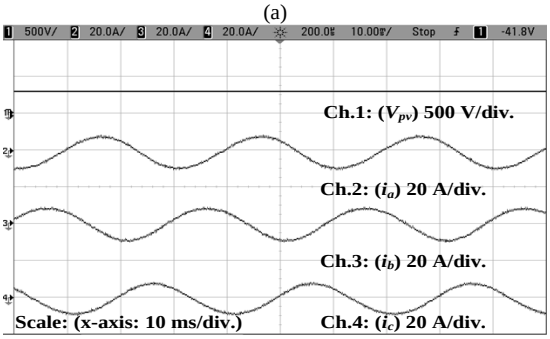

(b)

Fig. 18. Steady state performance (a)1000 W/m^2 (b) 500 W/m^2

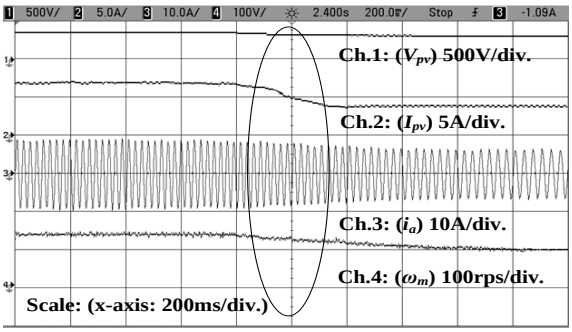

(a)

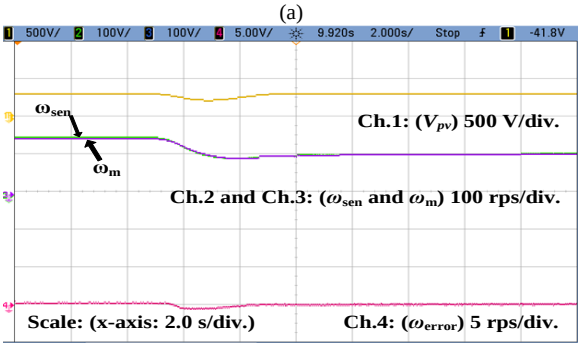

(b)

Fig. 19. Performance indices of (a) The proposed system (b) Waveforms showing sensed speed (ω_{sen}) and estimated speed (ω_m), during decrease in irradiance

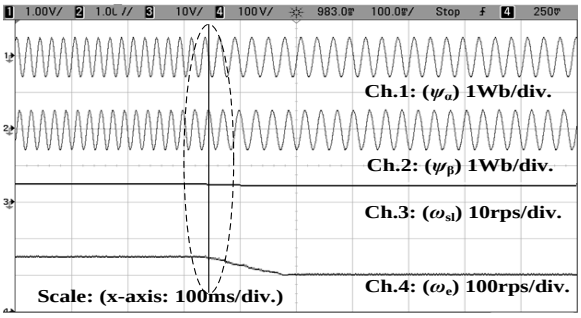

Fig. 20. Intermediate signals during step decrease in irradiance from 1000 W/m^2 to 500 W/m^2

This article has been accepted for publication in a future issue of this journal, but has not been fully edited. Content may change prior to final publication. Citation information: DOI 10.1109/TIA.2018.2810263, IEEE Transactions on Industry Applications

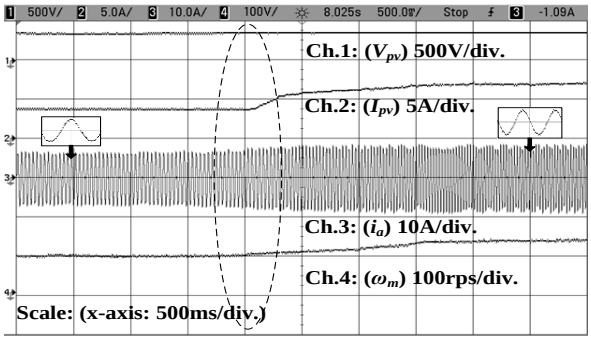

(a)

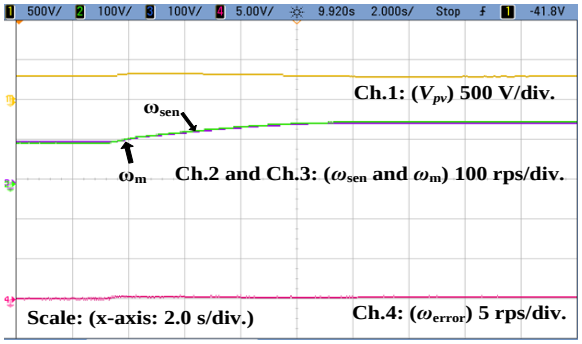

(b)

Fig. 21. Performance indices of (a) The proposed system (b) Waveforms showing sensed speed (ω_{sen}) and estimated speed (ω_m), during increase in irradiance

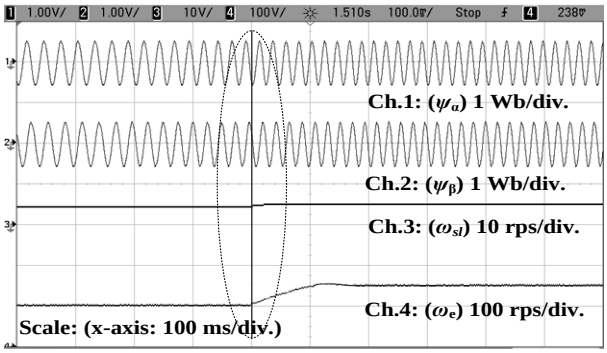

Fig. 22. Intermediate signals during step increase in irradiance from 1000 W/m^2 to 500 W/m^2

CONCLUSION

A single stage solar PV array fed speed sensorless vector-controlled induction motor drive has been operated subjected to different conditions and the steady state and dynamic behaviors have been found quite satisfactory and suitable for water pumping. The torque and stator flux, have been controlled independently. The motor is started smoothly. The reference speed is generated by DC link voltage controller controlling the voltage at DC link along with the speed estimated by the feed-forward term incorporating the pump affinity law. The power of PV array is maintained at maximum power point at the time of change in irradiance. This is achieved by using incremental-conductance based MPPT algorithm. The speed PI controller has been used to control the q-axis current of the motor. Smooth operation of IMD is achieved with desired torque profile for wide range of speed control. Simulation results have displayed that the controller behavior is found satisfactory under steady state and dynamic conditions of insolation change. The suitability of the drive is also verified by experimental results under various conditions and has been found quite apt for water pumping.

ACKNOWLEDGEMENT

The authors acknowledge the contribution and render their thankfulness to Dept. of Science and Tech. (DST), GoI for financing this project under Grant No.:RP02926.

APPENDICES

A. Solar PV Array (Simulation Data)

V_{oc}=760V, V_{mp}=600 V, I_{sc}=16 A, I_{mpp}=14.5 A, N_{ser}=34, N_{par}=25, (f_s)= 10 *k*Hz, DC-link Capacitor (C_{dc})= 2500 µF.

B. Solar PV Array (Experimental Data)

V_{oc}=400 V, V_{mp}=350 V, I_{sc}=8.4A, I_{mp}=7.2 A.

C. Induction Motor Parameters (Simulation Data)

7.5 kW (10 hP), 3-phase, 415 V (L-L), 2 poles, R_s=0.7384 Ω, L_{ls}= 0.003045 H, R_r= 0.7043 Ω, L_{lr}= 0.003045 H, L_m=0.1241 H, J=0.0343 Kg-m^2.

D. Induction motor parameters (Experimental Data)

2200W (3 hP), 3-phase, 230 V, 4 poles, R_s=0.603Ω, L_{ls}= 0.00293 H, R_r= 0.7 Ω, L_{lr}=0.00293H, L_m= 0.07503 H, J= 0.011Kg-m^2.

REFERENCES

[1] R. Foster, M. Ghassemi and M. Cota, Solar energy: Renewable energy and the environment, CRC Press, Taylor and francis Group, Inc. 2010.

[2] M. Kolhe, J. C. Joshi and D. P. Kothari, "Performance analysis of a directly coupled photovoltaic water-pumping system", *IEEE Trans. on Energy Convers.*, vol. 19, no. 3, pp. 613-618, Sept. 2004.

[3] J. V. M. Caracas, G. D. C. Farias, L. F. M. Teixeira and L. A. D. S. Ribeiro, "Implementation of a high-efficiency, high-lifetime, and low-cost converter for an autonomous photovoltaic water pumping system", *IEEE Trans. Ind. Appl.*, vol. 50, no. 1, pp. 631-641, Jan.-Feb. 2014.

[4] R. Kumar and B. Singh, " Buck-boost converter fed BLDC motor for solar PV array based water pumping, " *IEEE Int. Conf. Power Electron. Drives and Energy Sys. (PEDES)*, 2014.

[5] Zhang Songbai, Zheng Xu, Youchun Li and Yixin Ni, "Optimization of MPPT step size in stand-alone solar pumping systems," *IEEE Power Eng. Society Gen. Meeting*, June 2006.

[6] H. Gonzalez, R. Rivas and T. Rodriguez, "Using an artificial neural network as a rotor resistance estimator in the indirect vector control of an induction motor," *IEEE Latin Amer. Trans (Revista IEEE America Latina)* , vol.6, no.2, pp.176-183, June 2008.

[7] S. K. Sahoo and T. Bhattacharya, "Field Weakening Strategy for a Vector-Controlled Induction Motor Drive Near the Six-Step Mode of Operation," *IEEE Trans. Power Electron.*, vol. 31, no. 4, pp. 3043-3051, April 2016.

[8] T. Esram and P.L. Chapman, "Comparison of photovoltaic array maximum power point technique," *IEEE Trans. Energy Convers.*, vol.22, no.2, pp.439-449, June 2007.

[9] F. Liu, S. Duan, F. Liu, B. Liu and Y. Kang, "A variable step size INC MPPT method for PV systems," *IEEE Trans. Ind. Electron.*, vol. 55, no. 7, pp. 2622-2628, July 2008.

[10] M. A. Elgendy, D. J. Atkinson and B. Zahawi, "Experimental investigation of the incremental conductance maximum power point tracking algorithm at high perturbation rates," *IET Renewable Power Generation*, vol. 10, no. 2, pp. 133-139, Feb. 2016.

[11] A. B. Raju, S. Kanik and R. Jyoti, "Maximum efficiency operation of a single stage inverter fed induction motor PV water pumping system", *Emerging Trends in Eng. And Tech. (ICETET)*, pp.905-910, 2008.

[12] C. Jain and B. Singh, "Single-phase single-stage multifunctional grid interfaced solar photo-voltaic system under abnormal grid conditions", *IET Genr., Trans. & Distr.*, vol. 9, no. 10, pp. 886-894, Feb.2015.

[13] S. Shukla and B. Singh, "Single stage SPV array fed speed sensorless vector control of induction motor drive for water pumping," *IEEE Int.*

Conf. Power Electron., Intelligent Control and Energy Systems (ICPEICES), 2016, pp. 1-6, 2016.

[14] J. Titus, J. Teja, K. Hatua and K. Vasudevan, "An Improved Scheme for Extended Power Loss Ride-Through in a Voltage-Source-Inverter-Fed Vector-Controlled Induction Motor Drive Using a Loss Minimization Technique," *IEEE Trans. Ind. Appl.*, vol. 52, no. 2, pp. 1500-1508, March-April 2016.

[15] S. A. Odhano, R. Bojoi, A. Boglietti, Ş. G. Roşu and G. Griva, "Maximum Efficiency per Torque Direct Flux Vector Control of Induction Motor Drives," *IEEE Trans. Ind. Appl.*, vol. 51, no. 6, pp. 4415-4424, Nov.-Dec. 2015.

[16] L. An and D. D. C. Lu, "Design of a single-switch DC/DC converter for a PV-battery-powered pump system with PFM+PWM control," in *IEEE Trans. Ind. Electron.*, vol. 62, no. 2, pp. 910-921, Feb. 2015.

[17] D. Stojić, M. Milinković, S. Veinović and I. Klasnić, "Improved stator flux estimator for speed sensorless induction motor drives," *IEEE Trans. Power Electron.*, vol. 30, no. 4, pp. 2363-2371, April 2015.

[18] D. Casadei, G. Serra, A. Tani, L. Zarri and F. Profumo, "Performance analysis of a speed-sensorless induction motor drive based on a constant-switching-frequency DTC scheme," *IEEE Trans. Ind. Appl.*, vol. 39, no. 2, pp. 476-484, Mar/Apr 2003.

[19] B. Singh, G.Bhuvaneswari and V.Garg, "A Novel polygon based 18-pulse AC–DC converter for vector controlled induction motor drives," *IEEE Trans.Power Electron.*, vol.22, pp.488-497, March 2007.

[20] R. Kumar, S. Das, P.Syam and A.K. Chattopadhyay, "Review on model reference adaptive system for sensorless vector control of induction motor drives," *IET Elec. Power Appl.*, vol.9, pp.496-511, Aug. 2015.

[21] W. V. Jones, "Motor selection made easy: Choosing the right motor for centrifugal pump applications," *IEEE Ind. Appl. Mag.*, vol. 19, no. 6, pp. 36–45, Nov./Dec. 2013.

Saurabh Shukla was born in Andal (W.B), India, in 1988. He received the B.Tech. degree in Electrical Engineering from Asansol Engineering College (WBUT), Post Graduate Diploma Course in Thermal Power Plant Enginnering from National Power Training Institute (N.P.T.I) Nangal in 2012 and M.Tech. degree in Instrumentation and Control Enginnering from the Sant Longowal Institute of Engineering and Technology (SLIET) Sangrur, Punjab in 2014. He is currently working toward the Ph.D. degree in the Department of Electrical Engineering, Indian Institute of Technology Delhi. His areas of research interests include power electronics, electrical machines and drives, and renewable energy.

Bhim Singh (SM'99, F'10) was born in Rahamapur, Bijnor (UP), India, in 1956. He received his B.E. (Electrical) from the University of Roorkee, India, in 1977 and his M.Tech. (Power Apparatus & Systems) and Ph.D. from the Indian Institute of Technology Delhi, India, in 1979 and 1983, respectively.

In 1983, he joined the Department of Electrical Engineering, University of Roorkee (Now IIT Roorkee), as a Lecturer. He became a Reader there in 1988. In December 1990, he joined the Department of Electrical Engineering, IIT Delhi, India, as an Assistant Professor, where he has become an Associate Professor in 1994 and a Professor in 1997. He has been ABB Chair Professor from September 2007 to September 2012. Since October 2012, he is CEA Chair Professor. He has been Head of the Department of Electrical Engineering at IIT Delhi from July 2014 to August 2016. Since, August 2016, he is the Dean, Academics at IIT Delhi. He is JC Bose Fellow of DST, Government of India since December 2015. Prof. Singh has guided 65 Ph.D. dissertations, 167 M.E./M.Tech./M.S.(R) theses, and 60 BE/B.Tech. Projects. He has been filed 23 patents. He has executed more than eighty sponsored and consultancy projects. He has co-authored a text book on power quality: *Power Quality Problems and Mitigation Techniques* published by John Wiley & Sons Ltd. 2015. His areas of interest include solar PV grid interface systems, microgrids, power quality monitoring and mitigation, solar PV water pumping systems, improved power quality AC-DC converters, power electronics, electrical machines, drives, FACTS, and high voltage direct current (HVDC) systems. Prof. Singh is a Fellow of the Indian National Academy of Engineering (FNAE), The Indian National Science Academy (FNA), The National Academy of Science, India (FNASc), The Indian Academy of Sciences, India (FASc), The World Academy of Sciences (FTWAS), Institute of Electrical and Electronics Engineers (FIEEE), the Institute of Engineering and Technology (FIET), Institution of Engineers (India) (FIE), and Institution of Electronics and Telecommunication Engineers (FIETE) and a Life Member of the Indian Society for Technical Education (ISTE), System Society of India (SSI), and National Institution of Quality and Reliability (NIQR). He has received Khosla Research Prize of University of Roorkee in the year 1991. He is recipient of JC Bose and Bimal K Bose awards of The Institution of Electronics and Telecommunication Engineers (IETE) for his contribution in the field of Power Electronics. He is also a recipient of Maharashtra State National Award of Indian Society for Technical Education (ISTE) in recognition of his outstanding research work in the area of Power Quality. He has received PES Delhi Chapter Outstanding Engineer Award for the year 2006. Professor Singh has received Khosla National Research Award of IIT Roorkee in the year 2013. He has also received Shri Om Prakash Bhasin Award-2014 in the field of Engineering including Energy & Aerospace. He has been the General Chair of the 2006 IEEE International Conference on Power Electronics, Drives and Energy Systems (PEDES'2006), General Co-Chair of the 2010 IEEE International Conference on Power Electronics, Drives and Energy Systems (PEDES'2010), General Co-Chair of the 2015 IEEE International Conference (INDICON'2015), General Co-Chair of 2016 IEEE International Conference (ICPS'2016) held in New Delhi.